THE JOURNAL OF PHYSICAL CHEMISTRY B

Article

pubs.acs.org/JPCB

Optical Properties of Triplex DNA from Time-Dependent Density Functional Theory

Tahereh Ghane,[†,‡] Giorgia Brancolini,[†] Daniele Varsano,[†,§] and Rosa Di Felice*[,†]

[†]Center S3, CNR Institute of Nanoscience, Via Campi 213/A, 41125 Modena, Italy

[‡]Department of Physics, University of Modena and Reggio Emilia, Via Campi 213/A, 41125 Modena, Italy

[§]Department of Physics, University of Rome "La Sapienza", Piazzale Aldo Moro 5, 00185 Rome, Italy

Supporting Information

ABSTRACT: We present a combined investigation of the dynamics and optics of triplex DNA, based on classical molecular dynamics and time-dependent density functional theory. Our approach is devised to include the effects of conformational fluctuations on the electronic structure and optical excitations of the system. We find that the structural flexibility has a strong role in the determination of the optical signals. Our results allow us to unravel the peculiar fingerprints of Watson–Crick and Hoogsteen H-bonding in the optical absorption spectra. We find a specific optical absorption feature that is due to the simultaneous presence of the two H-bonding patterns in C^+GC triplets. While this peculiar triplet signal is wiped out in some structures that are representative of the finite-temperature dynamics, it can be recovered in an average view, so that it is a pristine result of this work.

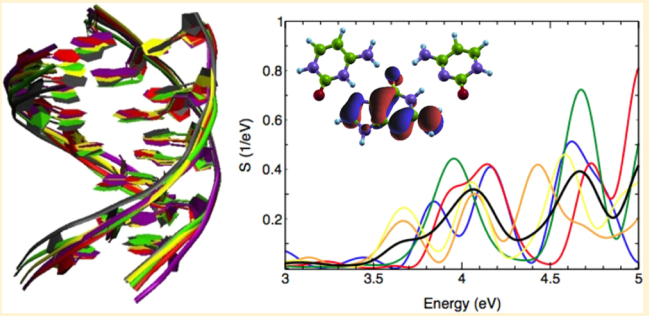

INTRODUCTION

Alterations of the composition and helical conformation of DNA are widely explored both for their biological implications and for their potential exploitation in new nanotechnologies.[1] Triplex DNA is a modified nucleic acid form in which three strands are connected to each other by hydrogen bonds. In particular, it can be obtained through the attachment, by Hoogsteen pairing, of a strand of pyrimidine bases to the purines of a Watson–Crick double-stranded DNA molecule, resulting in a structure with two different kinds of H-bonding motifs.[2] Thanks to their sequence-specificity and affinity, triplex-forming oligonucleotides have been proposed as a tool for gene targeting and have raised interest for antigene therapy.[3,4]

The hydrogen-bonding patterns in the adenine-thymine (AT) and guanine-cytosine (GC) base pairs have been studied using the density functional theory (DFT).[5,6] In a recent joint experiment–theory study,[7] it has been shown that the fingerprints of Watson–Crick and cross-strand/interplane hydrogen bonds can be discerned in the circular dichroism (CD) spectra of adenine tracts. The identification of the different H-bonding patterns was done by comparing the CD signals measured by synchrotron radiation to those computed by time-dependent density functional theory (TDDFT). Specifically, the experiments consisted of measuring CD spectra for several different double-stranded and single-stranded A-rich sequences and then performing a principal component analysis to identify the peaks due only to the pairing. The calculations were done for single Watson–Crick and cross-strand/interplane AT pairs, which, though different from the measured samples, are suitable to identify the sole features of the pairing and therefore to compare to the principal component analysis. The theoretical part of the work was able not only to interpret the experimental data in terms of electronic transitions, but also to exclude one particular form of cross-strand/interplane pairing that the experiments could not resolve.

Stimulated by this nice success and motivated by new synchrotron radiation optical experiments on triplex DNA,[8] we undertook a TDDFT investigation of C^+GC triplets with the objective of distinguishing the features of Watson–Crick and Hoogsteen pairing. While a joint analysis of the CD spectra is still under way and will deserve a separate publication, we devote our attention in this article to the optical absorption spectra and show that indeed in triplex DNA the two different kinds of H-bonds induce different transformations of the optical transitions and concurrent effects. The optical absorption spectrum can thus be used as a tool to detect the existence of triplex DNA.

Furthermore, in planning this study we realized that in the latest years there is more and more evidence that molecular flexibility plays a strong role in the optical properties and in the charge-transfer capabilities of nucleic acids.[9−14] Therefore, we did not restrict our TDDFT calculations to a single frozen geometry, but we adopted a hybrid classical-quantum computa-

Received: May 17, 2012
Revised: August 5, 2012
Published: August 6, 2012

tional strategy in which the quantum calculations are performed on structures derived from a classical molecular dynamics (MD) simulation of a triplex DNA oligomer in aqueous solvent at room temperature. The trajectory of the oligomer was sorted out to extract a limited number of representative structures, each of which was pruned to a single C^+GC triplet on which quantum calculations are affordable. We obtained results for five representative fragments and we discuss the relevance of the conformational flexibility in the optical absorption spectra.

Our hybrid methodology is similar in principle to that applied recently to single-stranded DNA[14] and natural dyes,[15] but this is the first time that the strategy has been extended to a modified DNA, with the necessity of ab initio-based force-field parametrization and the use of a sorting algorithm on the MD trajectory. Theoretical approaches for the identification of different H-bonding motifs go beyond the specific application disclosed here and have a huge potential to shed light on biological issues: for instance, it is known that either Watson–Crick[16] or Hoogsteen[17] H-bonds are found in AT pairs in the binding region of the transcription factor p53.

METHOD

The vast majority of DNA electronic structure calculations was performed so far on static structural fragments[18,19] that were either extracted from pdb files or constructed with nucleic acid builders on the basis of standard structural parameters (rise, twist, etc.). The role on the DNA electronic structure of the conformational changes, the interaction of the helix with the solvent, and the motion of counterions were neglected in these studies. However, recent work shows that the conformational and environmental effects on the electronic and optical properties of DNA and DNA derivatives can be crucial.[9−14]

There are various schemes proposed to take them into account. One possibility is to perform a quantum molecular dynamics (MD) simulation that directly gives the variability of the electro/optical properties in time at a finite temperature: because of the large system size, this is feasible only at the expense of the precision in the description of the electronic structure (essentially, by using tight-binding Hamiltonians).[12] We choose an alternative approach which allows us to retain a better accuracy in the electronic structure at the expense of the dynamical sampling. This multistep approach consists of the following steps: (i) setup of a viable initial structure that must be evolved in time at finite temperature; (ii) force-field generation (this is not always necessary, but it is essential in our triplex sequence that contains the nonconventional protonated cytosine); (iii) a classical molecular dynamics simulation of the DNA-derivative oligomer in explicit solvent; (iv) extraction of representative structures and pruning of manageable fragments; and (v) computation of the electronic structure and/or optical properties of such fragments that encompass the whole trajectory.

Molecular Dynamics. Molecular dynamics (MD) simulations were carried out using the NAMD program[20] with the AMBER force field.[21] Specifically, we used the parmbsc0 parametrization,[22] which is a refinement of the AMBER parm99 force field and is parametrized for proteins and nucleic acids. The 14-mer DNA triplex was built using the X3DNA package[23,24] with standard structural parameters[25] for the helical rise and the helical twist, 3.160 Å and 32.7°, respectively (including the third strand). It is constituted of a Watson–Crick poly(dG)-poly(dC) duplex connected by Hoogsteen H-bonds to a single strand of protonated cytosine (C^+). Although this sequence was never simulated before, the C^+GC triplet motif is known:[26] it is shown in Figure 1 with atomic labeling.

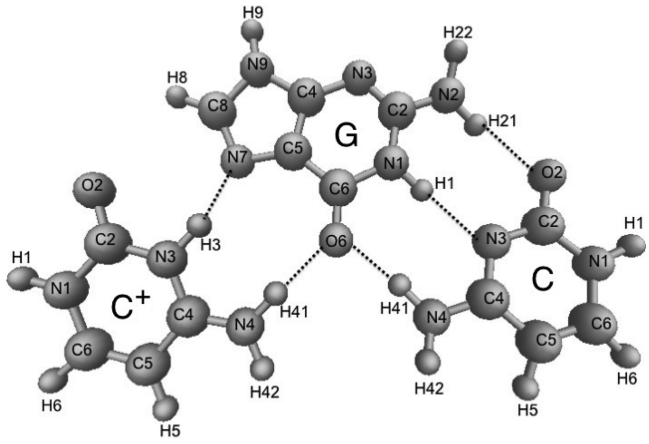

Figure 1. The triplet motif with definition of atomic labels. The two different kinds of hydrogen bonds are marked with dashed lines. G and C are paired by Watson–Crick H-bonding, and C^+ and G are paired by Hoogsteen H-bonding. The Watson–Crick base pairing between guanine and cytosine is characterized by three H-bonds: one between the carbonyl oxygen of guanine (O6) and the amino hydrogen of cytosine (H41), one between the N1H1 site of guanine and the N3 site of cytosine, and one between the amino hydrogen of guanine (H21) and the carbonyl oxygen of cytosine (O2). The Hoogsteen base pairing between protonated cytosine and guanine is characterized by two H-bonds: one between the carbonyl oxygen of guanine (O6) and the amino hydrogen of protonated cytosine (H41) and the other between the N7 site of guanine and the N3H3 site of protonated cytosine. Thus, in a C^+GC triplet, the O6 atom of the guanine base is engaged in two different H-bonds.

The triplex was located in the middle of a simulation box that is filled with TIP3P[27] water molecules for a thickness of about 16 Å from the DNA molecule in each direction. Na^+ and F^- counterions were present in the simulation box to neutralize the negative charges of the backbone and the positive charges of the protonated cytosines, respectively, thus ensuring the neutrality of the whole system. The choice of the anionic species is based on experimental setup.[8] The counterions do not aggregate during the dynamics.

We remark that the parmbsc0 AMBER force field that we adopted in the simulation does not contain parameters for protonated cytosine, which is present in the triplex-DNA oligomer that we wish to simulate. Therefore, we generated force field parameters for C^+ consistent with the AMBER force field. To this aim, we performed structural optimization and electronic structure calculations for the C^+GC triplet at two different levels of theory, namely HF/6-31G(d) and B3LYP/ccpVTZ, using the Gaussian03 computer package.[28] The missing bond and angle parameters for C^+ were built using the parmcal tool of the AMBER package, using the structures obtained from ab initio calculations. Charges were derived by fitting the ab initio ESP grid points[29,30] following the Merz–Kollman scheme, and from these a set of RESP (restrained electrostatic potential) atomic charges was derived. Short test MD simulations of the target triplex DNA over 5 ns gave similar results with these two parametrizations of C^+, in terms of stability of the triple helix as inspected by the analysis of partial and total root-mean-square deviations. Therefore, we chose to run the production MD simulation over longer times

dx.doi.org/10.1021/jp304818s | J. Phys. Chem. B 2012, 116, 10693−10702

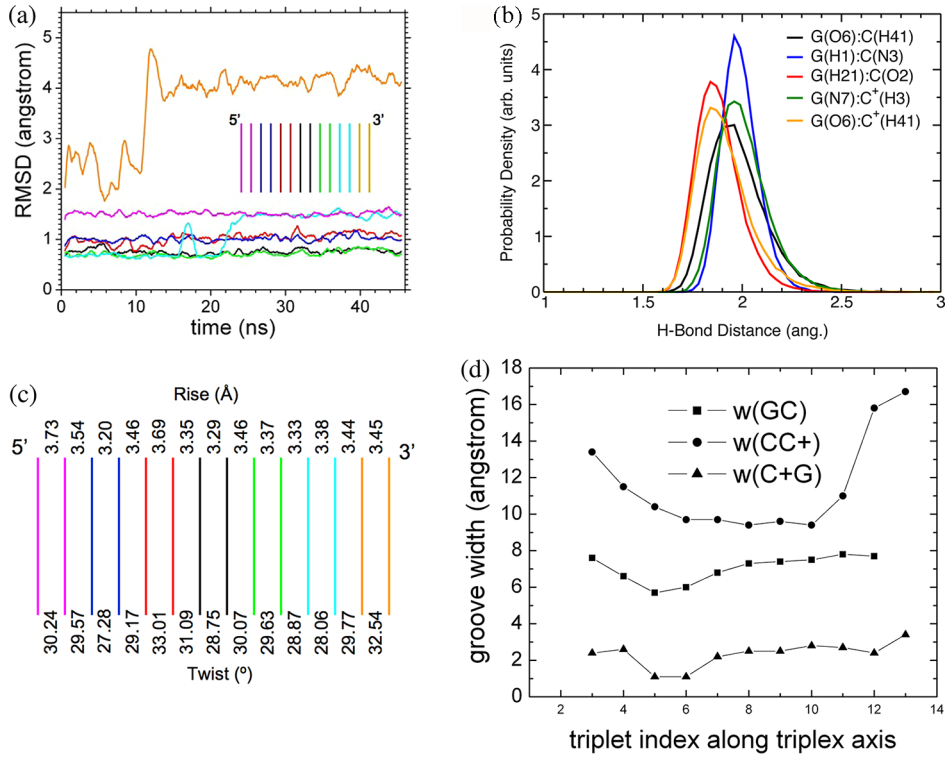

Figure 2. (a) Root mean square deviation as a function of simulation time for dimers of triplets in different portions of the 14-mer triplex. Black: central dimer. Red, blue, magenta: dimer 1, 2, 3 starting from the central dimer toward the 5′ end. Green, cyan, orange: dimer 1, 2, 3 starting from the central dimer toward the 3′ end. The inset is a cartoon of the stack of triplets, in which dimers of C^+GC triplets are represented in different colors that match the colors of the curves in the plot. The rmsd curves are smoothed over the range of 1 ns. The bare signals without smoothing are reported in the Supporting Information. (b) Statistics of the H-bonds distances in the 2 innermost C^+GC triplets. (c) Illustration of the interbase parameters rise and twist between any two C^+GC triplets along the triplex 14-mer. The color code is the same as in (a). (d) Plot of the groove width as a function of the location along the triplex 14-mer (1 is 5′, 14 is 3′).

with the parameters for C^+ obtained at the HF/6-31G(d) level, which is the default charge approach applied in the AMBER force field. The production MD run was preceded by a minimization−equilibration procedure, according to a well-established protocol.[31] The minimization was based on the conjugate gradient algorithm. The whole simulation was articulated in different steps. (1) We initially performed solvent equilibration only: all the water molecules and the cations were subjected to 20 ps dynamics, while the nucleic acid molecule was kept fixed with a SHAKE[32] tolerance of 10^{-8}. During this solvent equilibration, the temperature of the solvent molecules was slowly raised to 100 K by coupling to the heat bath and the pressure was kept fixed at 1.013 25 bar using the Berendsen method.[33] (2) We performed a full-atom minimization of this partially equilibrated system. (3) The quenched system was heated slowly from 0 to 300 K, by coupling it to a heat bath whose temperature was raised at the rate of 50 K every 10 ps. (4) The system was equilibrated 100 ps longer at the temperature and pressure of 300 K and 1.01325 bar, respectively. (5) Finally, we ran the production MD simulation of the 14-mer triplex-DNA molecule at the same temperature and pressure in the NPT ensemble, for 46 ns during which we collected the system coordinates every 1 ps.

The molecular dynamics trajectory can be used to account for the effect of structural fluctuation on the absorption spectra. In principle, this information could be achieved by calculating the optical spectra of the whole simulated oligomer at each snapshot and then averaging the signals. However, this is too computationally demanding for calculation of the optical properties at the TDDFT level, rather than with empirical methods. To enable TDDFT calculations, the size of the system and the number of significant structures must be reduced. Data-mining techniques, like clustering of structures by similarity, are efficient tools to sort out representative information from the whole trajectory.[34] We used a means-clustering algorithm for this work. Means clustering starts by choosing a collection of seed points, each of which constitutes an initial similarity set. The procedure then takes into account all other data points by measuring the root-mean-square deviation relative to the seed points. Each data point is assigned to the set whose centroid is closest and the centroid for this set is recomputed.[35] To provide greater consistency between runs, we chose as our initial points a collection of maximally distant seed points, although random collections can also be used. Using this algorithm within the Amber Tools package, groups of similar structures from different snapshots were produced based on the similarity of their conformations, which was evaluated in terms of root-mean-square deviation of the six central planes. For each group, a representative structure could be defined. Each representative structure was eventually pruned to a single C^+GC triplet. The TDDFT calculations were hence performed on such few representative triplets. In the next section we illustrate the representative oligomers and triplets and comment on the criteria for extraction of a triplet from each oligomer.

Optical Properties. Calculations of absorption spectra have been carried out by a real-time real-space implementation of time-dependent density functional theory[36,37] with the code

octopus.[38,39] In this method, the first step toward the computation of optical excitations is the determination of the ground state of the system, which is done at the DFT level. For the exchange-correlation potential we employed the local density approximation (LDA) with the Perdew−Zunger parametrization.[40] We used a real-space grid made of overlapping spheres with a radius of 5 Å centered around each nucleus. All quantities, including the wave functions, were discretized on a uniform grid with spacing 0.19 Å, both in the static DFT and in the time evolution.

After computing the ground state, an instantaneous electric-field perturbation $v(\mathbf{r},t) = -k_0 x_\nu \delta(t)$ was applied at time $t = 0$ and the Kohn−Sham orbitals were then evolved for a finite time. In the expression of the perturbation potential, $x_\nu = x,y,z$ indicates a Cartesian coordinate and k_0 is the intensity of the electric field, which should be small to maintain a dipolar regime: we used an electric field of 0.01 V in our calculations. In all the calculations we employed the adiabatic local density approximation (ALDA) and let each system evolve for a total time of $T = 33$ fs. The time step for the time evolution was 0.0066 fs, which guarantees the stability in the propagation of the Kohn−Sham wave functions.

From the Fourier transform of the real-time dipolar response to this perturbation, we then obtained the dynamical polarizability $\alpha_\nu(\omega)$ in the frequency range of interest. The dipole strength function $S_\nu(\omega)$ is obtained from the relation

$$S_\nu(\omega) = \frac{2m}{\pi p^2}\mathcal{F}\alpha_\nu(\omega) \tag{1}$$

The spatial average $S(\omega) = (1/3)\sum_\nu S_\nu(\omega)$ is proportional to the absorption cross section $\sigma(\omega)$ through the constant $2(\pi^2 p^2 \omega)/(mc)$, where m and c are the electron mass and the light velocity, respectively. $\sigma(\omega)$ is the quantity that is measured in experiments. Therefore, the computation of each polarized component of the dipolar strength function yields a signal that in principle can be directly compared with experimental data. This implementation of TDDFT also allows the calculation of circular dichroism spectra in a straightforward way.[41] For a more detailed description of this method, we refer the reader to specific articles.[38,39] This approach has already been used for the study of biomolecules,[42] including nucleic acids[10,43] and protein chromophores.[44−47]

RESULTS AND DISCUSSION

Structure and Stability of the Triplex. The root-mean-square deviation (rmsd) of the triplex with respect to the initial condition has been calculated for the entire oligomer and for portions of it. The backbone and H atoms were excluded from partial rmsds, while the total rmsd was computed with and without backbone and H atoms. The result of the equilibration phase was considered as the initial condition but we also checked the rmsd relative to the average conformation in the last 10 ns of the simulation (Supporting Information). The 46 ns MD trajectory reveals that the triplex structure remains stable against unfolding at constant temperature and pressure: no strand separation is observed during the dynamics, as revealed by the regular behavior of the total rmsd, which is presented in Figure S1 of the Supporting Information. Other authors[29,30,48] have simulated nucleic acid molecules containing three or four strands stabilized by C^+G Hoogsteen base pairs and found the stability of C^+GC triads. Our results are in agreement with such findings.

In Figure 2a we show how the comparison between the rmsd curves of dimer fragments computed in different portions of the 14-mer can reveal the most regular segments for pruning. The partial rmsd signals over dimers (Figure 2a) show that a significant amount of the total rmsd comes from the terminals of the triplex,[49] especially the 3′ terminal: in fact, the partial rmsd over dimers systematically increases going from the central dimer to the edge dimers and is particularly large at the 3′ terminal dimer. Therefore, we focused on the central portion of the oligomer to extract significant fragments for TDDFT calculations. In particular, we chose the triplet toward the 5′ terminal out of the two triplets in the central dimer.

The statistical distribution of H-bond length in the two central planes during the production MD simulations is presented in Figure 2b. The labels G(O6):C(H41), G(H1):C-(N3), and G(H21):C(O2) denote the Watson−Crick H-bonds, G(N7):C^+(H3) and G(O6):C^+(H41) denote the Hoogsteen H-bonds. The existence of relatively sharp single peaks reveals a good behavior of the H-bonds, which are preserved along the entire trajectory, in qualitative agreement with other simulations.[30] The average values are 1.93 ± 0.15 Å, 1.96 ± 0.09 Å, 1.84 ± 0.11 Å, 1.96 ± 0.12 Å, and 1.84 ± 0.10 Å, respectively. The statistics on the H-bond distances at terminal 3′ show disruption of the Hoogsteen H-bonds during the dynamics (see Supporting Information, Figure S4), which can be identified as the origin of the large rmsd at 3′ observed in Figure 2a.

Figure 2c,d illustrates the structural analysis of the trajectory, performed with CURVES+,[50] in terms of the interbase parameters rise and twist and of the widths of the grooves. In triplex DNA, as a consequence of the binding of the C^+ strand to the GC duplex, the major groove is divided into two parts: the Crick−Hoogsteen groove with width $w(C^+G)$ and the Watson−Hoogsteen groove with width $w(CC^+)$. The reported values in Figure 2c,d were obtained by averaging over time taking 1 snapshot every 1 ns, including the initial condition (a total of 47 snapshots). The rise and twist values are rather regular throughout the 14-mer. The mean values over the 14 planes of the oligomer are 3.44 ± 0.06 Å for the rise and 30 ± 1° for the twist. The rise from our MD trajectory is in the range 3.20−3.54 Å, with only slight exceptions on the 5′ side. This rise range is in good agreement with other theoretical results,[51] which suggested rise values between 3.3 and 3.5 Å. NMR data[52] indicate a rise value of 3.4 Å and twist values in the range 27−32°, which are also consistent with our results. Figure 2d shows that, by binding the third strand to the duplex, the width of the minor groove w(GC) is greatly reduced relative to B-DNA: in fact, we obtain a value of about 7 Å, rather constant through the stack, while the minor groove width of duplex B-DNA is 11.7 Å as determined by X3DNA. This rate of compression of the minor groove after formation the triplex was already reported by other authors.[53] Previous studies on triplex DNA structures[52,54−56] have shown that the groove widths $w(C^+G)$ and $w(CC^+)$ are essentially independent of sequence and are one-third and two-thirds, respectively, of the B-DNA duplex major groove width, which is 17.2 Å as determined by X3DNA. In contrast, we find a very small value for the width of the Hoogsteen-Crick groove $w(CC^+)$, most likely due to the presence of C^+ only in the third strand, which enhances electrostatic interactions and consequently shrinks the groove. This evidence points actually to a sequence dependence of the groove widths in triplex DNA, contrary to what previously concluded for a selection of sequences (T.AT, G.GC, TA.T,

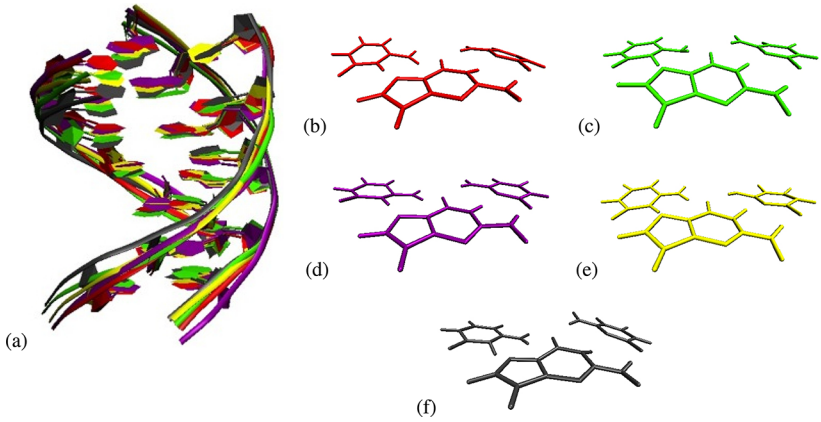

Figure 3. (a) Five representative structures selected from the MD trajectory on the basis of a clustering algorithm that groups structures, by similarity, namely by minimal deviation from each other. (b–f) The central triplet (without backbone) on the 5′ side, extracted from each representative structure: the same color code as in (a) is adopted. These fragments are the targets of our TDDFT calculations. Each representative oligomer, from which the triplets (b–f) are extracted, is populated by a fraction of the total number of MD snapshots equal to 11.90%, 22.95%, 20.73%, 22.56%, and 21.85%, respectively.

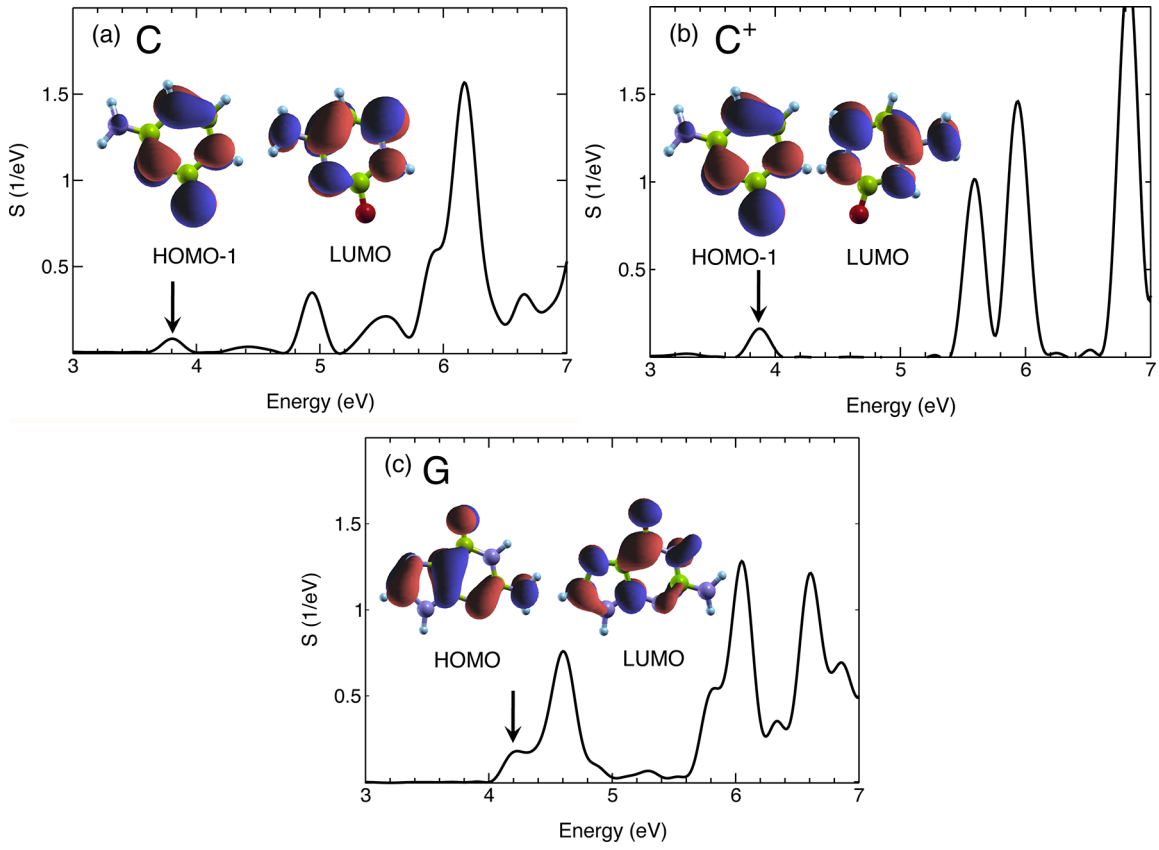

Figure 4. Dipolar strength function of isolated gas-phase (a) cytosine, (b) protonated cytosine, and (c) guanine, averaged over the three spatial directions. The inset in each panel shows the orbitals that define the transition associated to the lowest-energy peak (excluding charge-transfer excitations and non-$\pi\pi^*$ transitions), which is indicated by an arrow.

C^+.GC, G.TA, T.CG).[52,54−56] Indeed, sequence variations were also previously revealed, by comparing a C^+GC triplex to a TAT triplex.[53] The structure of the Crick−Hoogsteen groove is crucial for triplex stability. It is known that the low stability of triplexes is partially due to the strong electrostatic repulsion between the negatively charged phosphates that delimit this groove. For this reason, experiments have shown[57] that the thermodynamic stability of parallel DNA triple helices becomes increasingly pH dependent as the content of C^+GC triplets in the molecule is increased. The net stability at low pH increases in proportion to the number of C^+GC triplets.

In summary, the dynamics indicates that the triplex-DNA oligomer is fairly stable against disruption of the helix and that the central portion is the most regular, suitable for further analysis.

In Figure 3 we present the outcome of the clustering analysis and pruning of a minimal fragment. We sorted out five representative structures, which are shown in Figure 3a: while

dx.doi.org/10.1021/jp304818s | J. Phys. Chem. B 2012, 116, 10693−10702

all of them maintain the triplex motif, they exhibit clear differences that can be the origin of fluctuations in the optical signals. We noted above that the portion of the oligomer that is farthest from the terminals is the most regular. Therefore, we extracted a single C^+GC triplet from each representative structure by taking the seventh plane from the 5′ terminal and removing the backbone (the dangling bonds were capped by H atoms). These were the targets of our TDDFT calculations (see Figure 3b–f). We find structural differences between the representative triplets, due to dynamical fluctuations. Details are presented in the Supporting Information in terms of H-bond distances (Table S1) and intraplane translations and rotations (Table S2).

We are aware that these simple fragments do not contain all the characteristics of the oligomer, e.g., the solvent and the features due to stacking interactions. However, they are sufficient to reveal the fingerprints of Watson–Crick and Hoogsteen H-bonds and the differences between the two classes, which is the main objective of this study.

Optical Properties of C^+GC Triplets. In this section, we report the calculated optical absorption spectra for the triplets of Figure 3b–f. The interpretation of the optical spectrum for each triplet requires the comparison of the triplet signal to the signals of the component single bases and base pairs. In fact, we wish to identify if and where transitions characteristic of the individual components can be found in the triplet. We report here the complete result analysis for just one (Figure 3e) of the five selected triplets[58] and we discuss the importance of dynamical effects based only on the triplet spectra of all five structures. The full data for the other four structures are given in the Supporting Information (Figures S5–S20). We remind the reader that in these calculations we neglected the sugar–phosphate backbone. This simplification should not affect the energy range we are interested in, 3–6 eV: in fact, the sugar and phosphate contributions to the optical absorption signals of bases and base pairs are important only at higher energies. For instance, no backbone-induced features were detected below 6 eV in the optical conductivity of double-stranded DNA oligomers with different sequences computed by DFT.[59]

The computed dipolar strength functions, averaged over the three polarization directions, of the isolated cytosine, guanine, and protonated cytosine extracted from the triplet in Figure 3e are shown in Figure 4. The insets illustrate the transitions that mainly contribute to the lowest-energy peak in each panel. The real-time calculated energies of low-energy spectral peaks for the isolated bases extracted from the triplet of our pruned dynamical trajectory are reported in Table 1 (left column), along with some data from previous theoretical and experimental studies.[43,60−62] The comparison to other theoretical data is limited here to CIS[63] and CASPT2[60,61] data and to our previous work on GC pairs:[43] in the latter, the reader can find a detailed discussion of the work by other authors with various methods.[64−66] Table 1 and Figure 4 reveal considerable differences between neutral and protonated cytosine above 5 eV. However, we restrict our analysis to the lowest-energy peaks, which are instead quite similar in the two cytosine forms. The limitation to the energy range below 5 eV is suggested both by the higher interest in connection to experimental data and by the simplicity of analyzing optical modes to which just one or few electronic transitions contribute, as opposed to the high-energy peaks that include several transitions.

The performance of TDDFT relative to other ab initio methods and the agreement with experimental data was

Table 1. Vertical Excitation Energy (in eV) for the C^+GC Triplet, the Watson–Crick GC Pair, the Hoogsteen C^+G Pair, and the G, C, and C+ Bases[a,b]

this work	theory (TDDFT)[c]	CIS[d]	CASPT2[e]	expt[f]
		C^+GC Triplet		
3.67				
4.07				
4.43				
5.35				
5.82				
		GC Watson–Crick Pair		
4.06	4.29		4.35	
4.62	4.72		4.67	
		C^+G Hoogsteen Pair		
4.04				
4.63				
		G Base		
4.23	4.40	4.44		4.4–4.5
4.60	4.66	4.53	4.76	4.9–5.0
5.29	5.28	4.91	5.09	
5.83	5.76		5.96	5.7–5.8
		C Base		
3.80	4.18			4.6
4.42			4.39	
4.94	4.88			5.0–5.3
5.54			5.36	
5.94	5.80		6.16	5.4–5.8
		C^+ Base		
3.88				
5.59				

[a]The triplet, the pairs, and the bases of this work are frozen in the structure of Figure 3e. [b]We include in this table only the main peaks, while some other weak signals are mentioned in the text. [c]TDDFT data from Varsano and co-workers.[43] This work also discusses the effect of the environment: while the detailed comparison to experimental data depends on the solution conditions, basic effects for the identification of different optical features can be unraveled also in vacuum. [d]CIS data from Shukla and co-workers.[63] [e]CASPT2 data from Fulscher and co-workers.[60,61] [f]Experimental data are collected elsewhere.[60−62]

discussed by us elsewhere.[43] An overall glance at Table 1 reveals a fairly good agreement with other TDDFT results, except for a larger discrepancy in the first peak of cytosine. Since the method is exactly the same, we believe that the differences between our data and the results by Varsano and co-workers[43] are due to structural effects, because of the way we constructed our geometry to take into account fluctuations. To support this interpretation, data sets for triplets extracted from all five representative structures are included as Supporting Information: indeed, the scatter in the data confirms that structural fluctuations induce fluctuations of the peak energies in the optical absorption spectrum of single gas-phase bases and in H-bonded base complexes. Combining the time-domain spectra with the frequency domain analysis,[67] we can describe the spectral peaks in terms of transitions between electron states.

The first optical peak in the spectrum of cytosine at 3.80 eV has a $\pi\pi^*$ character. This fact was predicted in all recent computational studies.[43,64] We mainly focus here on $\pi\pi^*$ transitions, because the agreement of such transitions between different calculations and with experiment is typically much better than for other types of transitions. The second peak of

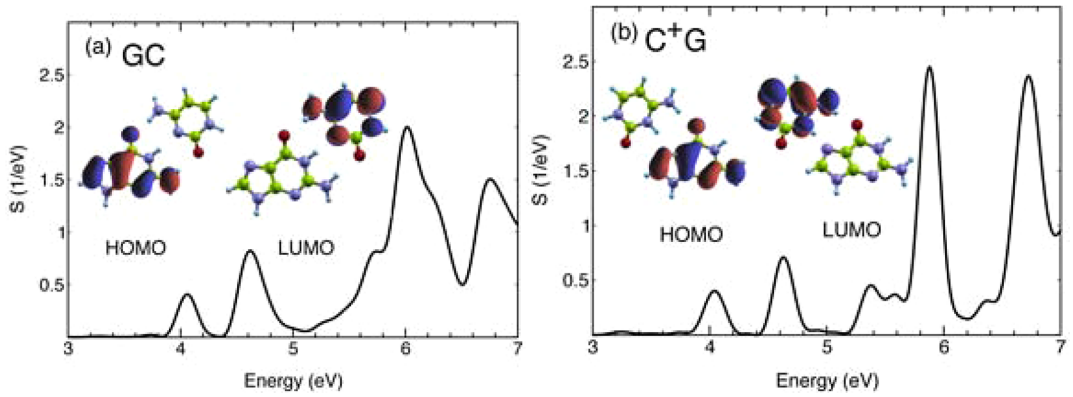

Figure 5. Average dipolar strength function of (a) GC and (b) C^+G calculated in this work by real-time propagation calculations. The inset in each panel illustrates HOMO and LUMO orbitals.

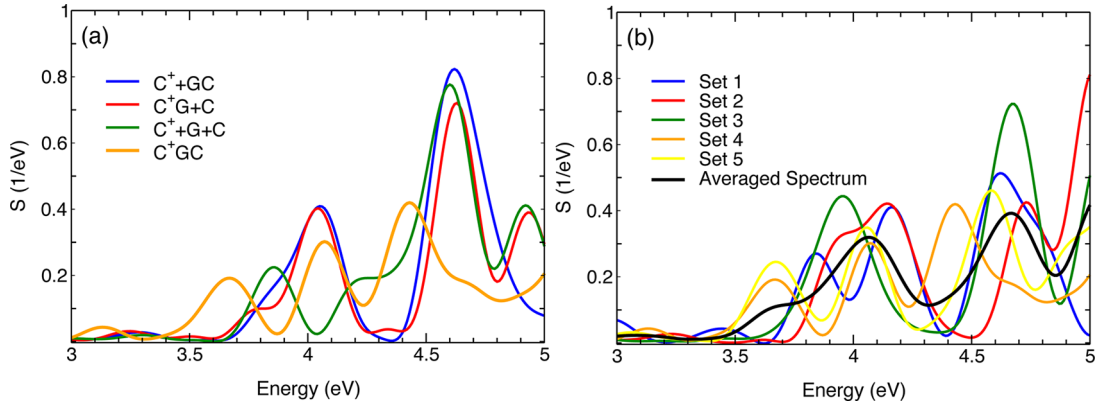

Figure 6. (a) Polarization-averaged dipolar strength function of the sample triplet in Figure 3a, plotted together with the superposition of component signals. The legend indicates the color code. (b) Polarization-averaged dipolar strength function of the five representative triplets, along with the average signal obtained by weighing the signal of each triplet with its population number during the dynamics.

cytosine at 4.42 eV has a mixed $\pi\pi^*-n\pi^*$ character: it is given by transitions from the HOMO-2 and HOMO-3 to the LUMO and from the HOMO to the LUMO+1 and LUMO+2. The spectrum of protonated cytosine, as compared to that of neutral cytosine, reveals an energy gap between 4 and 5.5 eV, where actually just a very weak peak is present at about 4.6 eV. The first peak of protonated cytosine at 3.88 eV corresponds to the same transition as the lowest-energy transition of cytosine found at 3.80 eV. Below this, an extra feature is found at 3.29 eV with an extremely low intensity: it corresponds to the transition between HOMO and LUMO, which has no equivalent in neutral cytosine at such low energies; it has a mainly $n\pi^*$ character, with a small percentage of $\pi\pi^*$ contribution; it cannot be detected in all the five representative structures (Supporting Information), which means that it is particularly sensitive to structural effects. The second peak of protonated cytosine at 5.59 eV has diverse traits, with the main contribution of $\pi\pi^*$ transitions. The first peak of guanine at 4.23 eV is related to the transition from the HOMO to the LUMO and LUMO+2. The second peak of guanine at 4.60 eV includes the transitions from HOMO-2 to LUMO and from HOMO to LUMO+1.

We now turn our attention to the Watson−Crick GC and Hoogsteen C^+G base pairs: a comparison between their optical absorption spectra allows us to characterize the fingerprints of the two different H-bonding schemes. Figure 5 shows the dipolar strength functions of GC and C^+G. The inset in each panel illustrates HOMO and LUMO. The energies of the spectral peaks are reported in Table 1.

The first peak in the GC spectrum at 4.06 eV has a $\pi\pi^*$ nature: it is the superposition between the first excitation of cytosine and the first excitation of guanine. The comparison between the GC pair and isolated G and C in Table 1 indicates that the effect of Watson−Crick hydrogen bonding is a blue shift by about 0.26 eV for the first cytosine peak and a red shift by about 0.17 eV for the first guanine peak. The second peak in the GC spectrum at 4.62 eV is a superposition between the second peak of guanine, slightly blue-shifted by 0.02 eV, and the second peak of cytosine, blue-shifted by 0.20 eV.

For the C^+G base pair, we find in Table 1 the first peak at 4.04 eV. The analysis of the transitions shows that this peak has a $\pi\pi^*$ nature and is produced by the superposition between the first excitation of protonated cytosine, blue-shifted by 0.16 eV, and the first excitation of guanine, red-shifted by 0.19 eV. Thus, Watson−Crick and Hoogsteen H-bonding are similar for what concerns the shift of the component peaks: they both give a red shift of the first guanine peak; they give a blue shift of the low-energy peaks of cytosine. The similarity of the spectra of the two base pairs suggests that the two kinds of H-bonding are hardly discernible in optical absorption measurements of double helices.[68] Yet, there is a more qualitative distinction between the two cases. Indeed, there is one extra excitation at 3.59 eV in the C^+G spectrum, not present in the GC spectrum, which is solely related to the protonated cytosine, without any purine composition: it has the same character as the weak low-

dx.doi.org/10.1021/jp304818s | J. Phys. Chem. B 2012, 116, 10693−10702

energy peak of C^+ at 3.29 eV. This is the main distinction that we find in the Hoogsteen pairing relative to the Watson−Crick pairing. The second peak of the C^+G spectrum at 4.63 eV has a mixed character: only the contribution from the second peak of guanine (slight blue shift by 0.03 eV) can be discerned clearly.

Not only the energy but also the oscillator strength of optical excitations is affected by H-bonding. The oscillator strengths of the first peak of isolated guanine and cytosine are 0.039 and 0.015, respectively, while the oscillator strength of the first peak of isolated protonated cytosine is 0.028. The G-peak oscillator strength remains practically equal in the Watson−Crick GC pair, where it is 0.038, but the C-peak oscillator strength significantly increases to 0.024. Instead, in the Hoogsteen C^+G pair, the G-peak is enhanced to a 0.043 oscillator strength and the first C^+-peak remains with a very similar strength, 0.027. Hence, the trends are slightly different for the two H-bonding schemes.

We now use the knowledge on the various transitions for single bases and base pairs to interpret the optical features of the C^+GC triplet. Figure 6a shows, for the sample structure of Figure 3e that we have examined also above, the triplet spectrum superimposed to the linear superpositions of the various components, in terms of only single bases or in terms of a base plus a pair. Figure 6b illustrates the dipolar strength functions for all the five C^+GC triplets extracted from our MD simulation and reported in Figure 3b−f.

The weak signal at 3.15 eV in the triplet spectrum in Figure 6a (orange line) corresponds to a charge-transfer excitation from guanine to protonated cytosine. The energy of charge-transfer excitations is greatly underestimated in TDDFT when local or semilocal exchange-correlation functionals are used[69−71] and therefore we do not elaborate on such transitions.

The first triplet peak with a $\pi\pi^*$ nature is at 3.67 eV: it is a superposition of the first excitation of cytosine and the first excitation of guanine, with a red shift by 0.13 and 0.56 eV relative to the isolated cytosine and guanine spectra, respectively. G and C are Watson−Crick paired in the C^+GC triplet, as they are in the GC pair, and the nature of the first triplet peak corresponds to that of the first peak of the GC pair. However, we note some differences in the peak shifts. The first guanine peak has a higher red shift in the triplet than in the pair. The first cytosine peak has even an inversion of the shift. These oddities are due to the simultaneous presence of the Hoogsteen H-bond in the triplet: in fact, the guanine is simultaneously engaged in both Watson−Crick and Hoogsteen H-bonding and therefore the interaction with cytosine is not exactly the same as in the GC pair. The global effect is that the combination of a Hoogsteen H-bond with a Watson−Crick H-bond induces a red shift by 0.39 eV on both the first C and the first G excitations, relative to their energies in the purely Watson−Crick GC pair.

The second peak of the C^+GC triplet at 4.07 eV has a mixed $\pi\pi^*-n\pi^*$ character and does not resemble any characteristics of either the GC or C^+G pair. In this peak, the fingerprint of the first excitation of protonated cytosine is clear: this is blue-shifted by 0.19 eV with respect to the isolated base. This peak also contains the transition from the HOMO-2 to the LUMO of guanine, which is one of the transitions that contribute to the second peak of the optical absorption spectrum of isolated guanine. The Kohn−Sham orbitals that mainly contribute to the first two absorption peaks in the C^+GC triplet are shown in Figure 7. The third peak at 4.43 eV has a mixed nature

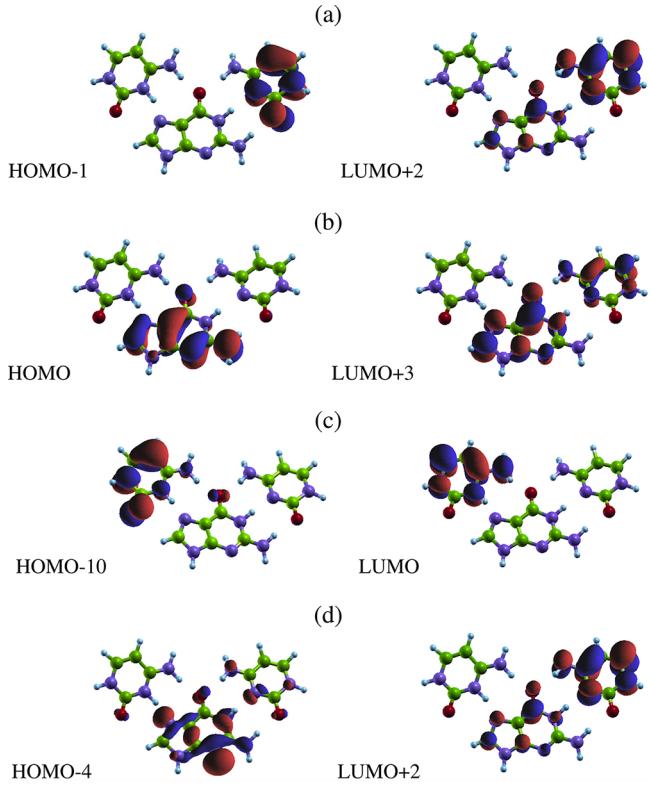

Figure 7. Isosurfaces of Kohn−Sham orbitals of the C^+GC triplet that contribute to the low-energy optical absorption peaks of Figure 6a. (a,b) The electronic transitions between these orbitals, from occupied to unoccupied, are the major components of the triplet peak at 3.67 eV. (c,d) The electronic transitions between these orbitals, from occupied to unoccupied, are the major components of the triplet peak at 4.07 eV. The contribution of other transitions in these two peaks is negligible.

composed of the second peak of cytosine, the second peak of guanine, and partial contribution of second peak of protonated cytosine. We note that the HOMO-2 → LUMO transition of andguanine, which is the main transition involved in the second excitation of isolated guanine, contributes in the triplet to two different excitations, namely at 4.07 and 4.43 eV. This behavior is due to the fact that the guanine base is simultaneously engaged in two different kinds of hydrogen bond.

The first two main peaks in the spectrum of the triplet in Figure 6a (orange line) cannot be considered as a superposition of the first peaks of the purely Watson−Crick and Hoogsteen pairs, because the nature of the second peak in the triplet spectrum is similar to neither the first peak of GC nor the first peak of C^+G. These two peaks can be interpreted by inspecting the different spectra of Figure 6a: the blue line is the sum of the absorption spectra of an isolated C^+ and an isolated WC GC pair, the red line is the sum of the absorption spectra of an isolated C and an isolated Hoogsteen C^+G pair, and the green line is the sum of the absorption spectra of isolated C^+, G, and C bases. The comparison between the different lines in Figure 6a gives insight on the effect of H-bonding. Specifically, we detect a peculiar peak splitting in the low-energy range in the triplet spectrum. In both the blue and red lines, which contain the effect of only one kind of H-bonding (WC in the blue line, Hoogsteen in the red line), we note the existence of a peak at 4 eV, with a low-energy shoulder due to the C and C^+ signals. Instead, in the orange line of the triplet there is a full peak

dx.doi.org/10.1021/jp304818s | J. Phys. Chem. B 2012, 116, 10693−10702

splitting: this feature, which is due to the appearance of new transitions as noted above, is a fingerprint of the simultaneous presence of the two H-bonding motifs.

In Figure 6b we present the effect of structural fluctuations on the absorption spectra of the triplets. Different representative triplets have different spectra characterized by energy shifts, which means that the description of structure and environment are important to interpret optical signals from real experiments. The peculiar peak splitting that we identified above as an optical fingerprint of the C^+GC triplet is indeed found repeatedly in the various triplets but not exactly in all of them. However, it is recovered in the average description (black line) and therefore should be detectable in optical measurements.

SUMMARY AND OUTLOOK

We have presented and discussed the results of a combined MD+TDDFT computational study of the optical absorption spectra of triplex DNA. We have analyzed the optical peaks in terms of orbital transitions. We find that protonated cytosine gives origin to a peculiar transition and that the simultaneous presence of Hoogsteen and WC H-bonding in a C^+GC triplet induces energy shifts and changes of intensities that are different than in GC and C^+G pairs in which a single type of H-bonding exists. Our results also show that optical absorption spectra are very sensitive to the structure, which implies that the molecular flexibility in a realistic environment cannot be neglected to attain predictive interpretation of experimental situations. The existence of mixed triplets C^+GC and C(imino)GC has been suggested.[51] The methodology adopted in our work can shed light on this issue, which is an appealing objective for future work.

We believe that this work outlines a valid reliable methodology for the investigation of the electronic and optical properties of natural and modified DNAs. We are confident that the comparison to measured CD spectra will eventually further validate our approach and theoretical understanding.

ASSOCIATED CONTENT

Supporting Information

Smoothed versus nonsmoothed rmsd curves. Structural analysis of the MD trajectory. Optical spectra and main transitions for all the representative structures extracted from the MD trajectory. This material is available free of charge via the Internet at http://pubs.acs.org.

AUTHOR INFORMATION

Corresponding Author

*E-mail: rosa.difelice@unimore.it.

Notes

The authors declare no competing financial interest.

ACKNOWLEDGMENTS

We are grateful to Angel Rubio, Anne Holm, and Steen Brøndsted Nielsen for stimulating this work, and to Anna Garbesi and Elisa Molinari for continuous fruitful discussions on related topics. The ISCRA staff at CINECA (Bologna, Italy) is acknowledged for computational facilities and technical support. This work was funded by the European Commission through project "DNA-Nanodevices" (contract no. FP6-029192) and through the Infrastructure e-I3 ETSF (contract no. INFRA-2007-1.2.2 "ETSF" 211956), by the ESF through COST Action MP0802, by the Italian Institute of Technology through project MOPROSURF and the Computational Platform. R.D.F. is also grateful to Remo Rohs for comments on this work and possible developments and to Fondazione Cassa di Risparmio di Modena for partial funding through Progetto Internazionalizzazione 2011.

REFERENCES

(1) Porath, D.; Cuniberti, G.; Di Felice, R. *Top. Curr. Chem.* **2004**, *237*, 183−227.
(2) Frank-Kamenetskii, M. D.; Mirkin, S. M. *Annu. Rev. Biochem.* **1995**, *64*, 65−95.
(3) Knauert, M. P.; Glazer, P. M. *Hum. Mol. Genet.* **2001**, *10*, 2243−2251.
(4) Singhal, G.; Akhter, M. Z.; Stern, D. F.; Gupta, S. D.; Ahuja, A.; Sharma, U.; Jagannathan, N. R.; Rajeswari, M. R. *Cancer Gene Ther.* **2011**, *18*, 520−530.
(5) Mallajosyula, S. S.; Datta, A.; Pati, S. K. *Synth. Met.* **2005**, *155*, 398−401.
(6) Mohan, P. J.; Datta, A.; Mallajosyula, S.; Pati, S. K. *J. Phys. Chem. B* **2006**, *110*, 18661−18664.
(7) Nielsen, L. M.; Holm, A. I. S.; Varsano, D.; Kadhane, U.; Hoffmann, S. V.; Di Felice, R.; Rubio, A.; Nielsen, S. B. *J. Phys. Chem. B* **2009**, *113*, 9614−9619.
(8) Holm, A. I. S.; Nielsen, S. B. Private communication.
(9) Migliore, A.; Corni, S.; Varsano, D.; Klein, M. L.; Di Felice, R. *J. Phys. Chem. B* **2009**, *113*, 9402−9415.
(10) Varsano, D.; Garbesi, A.; Di Felice, R. *J. Phys. Chem. B* **2007**, *111*, 14012−14021.
(11) Troisi, A.; Orlandi, G. *J. Phys. Chem. B* **2002**, *106*, 2093−2101.
(12) Kubař, T.; Woiczikowski, B.; Cuniberti, G.; Elstner, M. *J. Phys. Chem. B* **2008**, *112*, 7937−7947.
(13) Kubař, T.; Elstner, M. *J. Phys. Chem. B* **2008**, *112*, 8788−8798.
(14) Tonzani, S; Schatz, G. C. *J. Am. Chem. Soc.* **2008**, *130*, 7607−7612.
(15) Malcioglu, O. B.; Calzolari, A.; Gebauer, R.; Varsano, D.; Baroni, S. *J. Am. Chem. Soc.* **2011**, *133*, 15425−15433.
(16) Chen, Y.; Dey, R.; Chen, L. *Structure* **2010**, *18*, 246−256.
(17) Kitayner, M.; Rozenberg, H.; Rohs, R.; Suad, O.; Rabinovich, D.; Honig, B.; Shakked, Z. *Nat. Struct. Mol. Biol.* **2010**, *17*, 423−430.
(18) Sponer, J.; Leszczynski, J.; Hobza, P. *Biopolymers* **2002**, *61*, 3−31.
(19) Sponer, J.; Jurecka, P; Marchan, I.; Luque, F. J.; Orozco, M.; Hobza, P. *Chem.—Eur. J.* **2006**, *12*, 2854−2865.
(20) Phillips, J. C.; Braus, R.; Wang, W.; Gumbart, J.; Tajkhorshid, E.; Villa, E.; Chipot, C.; Skeel, R. D.; Kalé, L.; Schulten, K. *J. Comput. Chem.* **2005**, *26*, 1781−1802.
(21) Cornell, W. D.; Cieplak, P.; Bayly, C. I.; Gould, I. R.; Merz, K. M.; Ferguson, D. M.; Spellmeyer, D. C.; Fox, T.; Caldwell, J. W.; Kollman, P. A. *J. Am. Chem. Soc.* **1995**, *117*, 5179−5197.
(22) Pérez, A.; Marchán, I.; Svozil, D.; Sponer, J.; Cheatham, T. E., III; Laughton, A.; Orozco, M. *Biophys. J.* **2007**, *92*, 3817−3829.
(23) Lu, X.-J.; Olson, W. K. *Nucleic Acids Res.* **2003**, *31*, 5108−5121.
(24) The X3DNA code is available at http://3dna.rutgers.edu/x3dna/faqs.
(25) Arnott, S. Polynucleotide secondary structure: a historical perspective In *Oxford Handbook of Nucleic Acid Structure*; Neidle, S., Ed.: Oxford Press: Oxford, UK, 1999; pp 1−38.
(26) Chan, P. P.; Glazer, P. M. *J. Mol. Med.* **1997**, *75*, 267−282.
(27) Jorgensen, W. L.; Chandrasekhar, J.; Madura, J. D.; Impey, R. W.; Klein, M. L. *J. Chem. Phys.* **1983**, *79*, 926−935.
(28) Frisch, M. J.; Trucks, G. W.; Schlegel, H. B.; Scuseria, G. E.; Robb, M. A.; Cheeseman, J. R.; Montgomery, J. A., Jr.; Vreven, T.; Kudin, K. N.; Burant, J. C.; et al. *Gaussian 03, revision C.02*; Gaussian, Inc.: Wallingford, CT, 2004.
(29) Spackova, N.; Berger, I.; Egli, M.; Sponer, J. *J. Am. Chem. Soc.* **1998**, *120*, 6147−6151.

(30) Csaszar, K.; Spackova, N.; Stefl, R.; Sponer, J.; Leontis, N. B. *J. Mol. Biol.* **2001**, *313*, 1073−1091.
(31) Cavallari, M.; Calzolari, A.; Garbesi, A.; Di Felice, R. *J. Phys. Chem. B* **2006**, *110*, 26337−26348.
(32) Ryckaert, J. P.; Ciccotti, G.; Berendsen, H. J. C. *J. Comput. Phys.* **1997**, *23*, 327−341.
(33) Berendsen, H. J. C.; Postma, J. P. M.; van Gunsteren, W. F.; DiNola, A.; Haak, J. R. *J. Chem. Phys.* **1984**, *81*, 3684−3690.
(34) Torda, A. E.; Van Gunsteren, W. F. J. *Comput. Chem.* **1994**, *15*, 1331−1340.
(35) Shao, J.; Tanner, S. W.; Thompson, N.; Cheatham, T. E. J. *Chem. Theor. Comput.* **2007**, *3*, 2312−2334.
(36) Gross, E. K. U.; Dobson, J. F.; Petersilka, M. *Top. Curr. Chem.* **1996**, *181*, 81−172.
(37) Marques, M. A. L., Ullrich, C. A., Nogueira, F., Rubio, A., Burke, K., Gross, E. K. U., Eds. *Time Dependenent Density Functional Theory*; Springer: Berlin, 2006; Lect. Notes Phys., Vol. *706*, pp 197−215.
(38) Marques, M. A. L.; Castro, A.; Bertsch, G. F.; Rubio, A. *Comput. Phys. Commun.* **2003**, *151*, 60−78.
(39) Castro, A.; Appel, H.; Oliveira, M.; Rozzi, C. A.; Andrade, X.; Lorenzen, F.; Marques, M. A. L.; Gross, E. K. U.; Rubio, A. *Phys. Status Solidi B* **2006**, *243*, 2465−2488. The code OCTOPUS is available at http://www.tddft.org/programs/octopus/
(40) Perdew, J.; Zunger, A. *Phys. Rev. B* **1981**, *23*, 5048−5079.
(41) Varsano, D; Espinosa-Leal., L. A.; Andrade, X.; Marques, M. A. L.; Di Felice, R.; Rubio, A. *Phys. Chem. Chem. Phys.* **2009**, *11*, 4481−4489.
(42) Castro, A.; Marques, M. A. L; Varsano, D.; Sottile, F.; Rubio, A. *Compte Rendus Physique* **2009**, *10*, 469−490.
(43) Varsano, D.; Di Felice, R.; Marques, M. A. L.; Rubio, A. *J. Phys. Chem. B* **2006**, *110*, 7129−7138.
(44) Marques, M. A. L.; Lopez, X.; Varsano, D.; Castro, A.; Rubio, A. *Phys. Rev. Lett.* **2003**, *90*, 258101−258104.
(45) Lopez, X.; Marques, M. A. L.; Castro, A.; Rubio, A. *J. Am. Chem. Soc.* **2005**, *127*, 12329−12337.
(46) Cai, D.; Marques, M. A. L.; Milne, B. F.; Nogueira, F. *J. Phys. Chem. Lett.* **2010**, *1*, 2781−2787.
(47) Cai, D.; Marques, M. A. L.; Nogueira, F. *J. Phys. Chem. B* **2011**, *115*, 329−332.
(48) Basye, J.; Trent, J. O.; Gao, D. Q.; Ebbinghaus, S. W. *Nucleic Acids Res.* **2001**, *29*, 4873−4880.
(49) Weerasinghe, S.; Smith, P. E.; Mohan, V.; Cheng, Y. K.; Pettitt, B. M. *J. Am. Chem. Soc.* **1995**, *117*, 2147−2158.
(50) Lavery, R.; Moakher, M.; Maddocks, J. H.; Petkeviciute, D.; Zakrzewska, K. *Nucleic Acids Res.* **2009**, *37*, 5917−5929.
(51) Soliva, R.; Laughton, C. A.; Javier Luque, F.; Orozco, M. *J. Am. Chem. Soc.* **1998**, *120*, 11226−11233.
(52) Radhakrishnan, I.; Patel, D. J. *Structure* **1994**, *2*, 17−32.
(53) Asensio, J. L.; Brown, T.; Lane, A. N. *Structure* **1998**, *7*, 1−11.
(54) Radhakrishnan, I.; Patel, D. J. *Structure* **1993**, *1*, 135−152.
(55) Ji, J.; Hogan, M. E.; Gao, X. *Structure* **1996**, *4*, 425−435.
(56) Tarkoy, M.; Phipps, K.; Schultze, P.; Feigon, J. *Biochemistry* **1998**, *37*, 5810−5819.
(57) Plum, G. E.; Breslauer, K. J. *J. Mol. Biol.* **1995**, *248*, 679−695.
(58) Three of the five structures give very similar optical absorption signals. Among these, we present data for the one that has the largest occurrence during the dynamics and simultaneously yelds the best agreement with existing data for the isolated bases cytosine and guanine.
(59) Hübsch, A.; Endres, R. G.; Cox, D. L.; Singh, R. R. P. *Phys. Rev. Lett.* **2005**, *94*, 178102−178105.
(60) Fulscher, M. P.; Roos, B. *J. Am. Chem. Soc.* **1995**, *117*, 2089−2095.
(61) Fulscher, M. P.; Serrano-Andres, L.; Roos, B. *J. Am. Chem. Soc.* **1997**, *119*, 6168−6176.
(62) Tsolakidis, A.; Kaxiras, E. *J. Phys. Chem. A* **2005**, *109*, 2373−2380.
(63) Shukla, M. K.; Mishra, S. K.; Kumar, A.; Mishra, P. C. *J. Comput. Chem.* **2000**, *21*, 826−846.
(64) Shukla, M. K.; Leszczynski, J. *J. Phys. Chem. A* **2002**, *106*, 11338−11346.
(65) Shukla, M. K.; Leszczynski, J. *J. Comput. Chem.* **2004**, *25*, 768−778.
(66) Lorentzon, J.; Fulscher, M. P.; Roos, B. *J. Am. Chem. Soc.* **1995**, *117*, 9265−9273.
(67) Casida, E. In *Recent Advances in Density Functional Methods Part I*; Chong, D. P., Ed.; World Scientific: Singapore, 1995; pp 115−193.
(68) Mallajosyula, S. S.; Pati, S. K. *J. Phys. Chem.* **2007**, *111*, 11614−11618.
(69) Dreuw, A.; Weisman, J. L.; Head-Gordon, M. *J. Chem. Phys.* **2003**, *119*, 2943−2946.
(70) Dreuw, A.; Weisman, J. L.; Head-Gordon, M. *J. Am. Chem. Soc.* **2004**, *126*, 4007−4016.
(71) Gritsenko, O.; Baerends, E. J. *J. Chem. Phys.* **2003**, *121*, 655−660.